Collective Radiation of a Cascaded Quantum System: From Timed Dicke States to Inverted Ensembles

Christian Liedl, Sebastian Pucher, Felix Tebbenjohanns, Philipp Schneeweiss, and Arno Rauschenbeutel[*]

Department of Physics, Humboldt-Universität zu Berlin, 10099 Berlin, Germany

The collective absorption and emission of light by an ensemble of atoms is at the heart of many fundamental quantum optical effects and the basis for numerous applications. However, beyond weak excitation, both experiment and theory become increasingly challenging. Here, we explore the regimes from weak excitation to inversion with ensembles of up to 1000 atoms that are trapped and optically interfaced using the evanescent field surrounding an optical nanofiber. We realize full inversion, with about 80% of the atoms being excited, and study their subsequent radiative decay into the guided modes. The data are very well-described by a simple model that assumes a cascaded interaction of the guided light with the atoms. Our results contribute to the fundamental understanding of the collective interaction of light and matter and are relevant for applications ranging from quantum memories to sources of nonclassical light to optical frequency standards.

The collective emission of radiation by an ensemble of atoms is a central problem in quantum optics that has recently seen renewed interest in the context of optical quantum technologies. The super- and subradiant states that emerge when a propagating light field couples to a spatially extended ensemble of emitters can be used as a resource to implement novel protocols, e.g., in the context of quantum information, quantum communication, and frequency standards [1–5]. The underlying, so-called timed Dicke regime has been extensively studied, both theoretically and experimentally, e.g., with ensembles of laser-cooled atoms in the optical domain [6–14]. However, the regime where the ensemble is highly excited or even fully inverted has only recently become accessible [15–18]. There, the theoretical description becomes increasingly complex due to the exponential scaling of the system's Hilbert space with the number of emitters [19–25]. Nanofiber-based atom-light interfaces are a new experimental avenue for studying collective radiative dynamics, where all waveguide-coupled atoms couple efficiently to the guided optical mode [26–33]. In addition, direction-dependent coupling can be implemented, providing access to the field of chiral quantum optics [34], and the waveguide mediates an effectively infinite-range interaction between atoms [29,35–38]. While such systems have been explored in the weak excitation regime, coherent optical control and inversion of atomic ensembles coupled to nanophotonic structures have proven difficult [39]. This is due to comparably large passive heating rates, strong field gradients, and undesired spin-motion coupling.

Here, we explore the collective radiation of an ensemble of up to 1000 waveguide-coupled atoms from weak excitation to almost full inversion. The atoms are trapped close to an optical nanofiber and excited by a resonant, fiber-guided probe pulse that is much shorter than the excited state lifetime. We observe Rabi oscillations of the ensemble by counting the number of photons absorbed from the excitation pulse and achieve almost full inversion. We measure the fluorescence emitted into the nanofiber-guided modes, infer a collective coupling efficiency, and study its dependence on the pulse area and on the number of atoms. The almost unidirectional atom-waveguide coupling inherent to our system realizes a cascaded quantum system, allowing us to understand the dynamics by a model, whose complexity scales only linearly with the number of atoms. We note that superradiance in a cascaded quantum system is fundamentally different from superradiance on a cascade transition as, e.g., observed in Ref. [40].

Our experimental setup is schematically shown in Fig. 1(a). The nanofiber is realized as the waist of a tapered optical fiber and has a nominal diameter of 500 nm. A running-wave blue-detuned nanofiber-guided field (wavelength 760 nm, power 20.5 mW) and a standing-wave red-detuned field (wavelength 1064 nm, total power 2.4 mW) form two diametral arrays of optical trapping sites, located about 230 nm from the nanofiber surface. We prepare cesium atoms on only one side of the fiber with at most one atom per trapping minimum [41–44]. We choose the quantization axis $(+z)$ to be normal to the plane formed by the array of atoms and the nanofiber. We then infer the number of trapped atoms, N, using transmission spectroscopy [42]. Throughout the experimental sequence described below, we continuously perform degenerate Raman cooling of the optically trapped atoms on the $|6S_{1/2}, F = 4\rangle \rightarrow |6P_{1/2}, F = 4\rangle$ D1 transition. The scattering rate of this free-space laser field is far
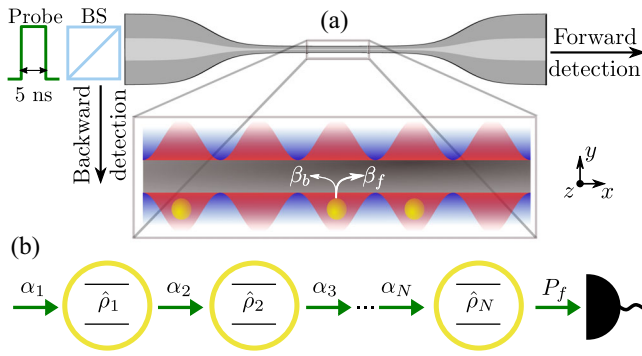
FIG. 1. (a) Schematic of the experimental setup. Cesium atoms (yellow discs) in a nanofiber-based dipole trap are evanescently interfaced with a guided probe pulse. The atom-waveguide coupling strengths β_f and β_b are propagation-direction-dependent, indicated by the white arrows. The transmitted and reflected pulses are sent to two detection setups. (b) We model the system dynamics using a cascaded interaction model, where the kth atom is described by the density operator $\hat{\rho}_k$ and is driven by a coherent field with amplitude α_k.
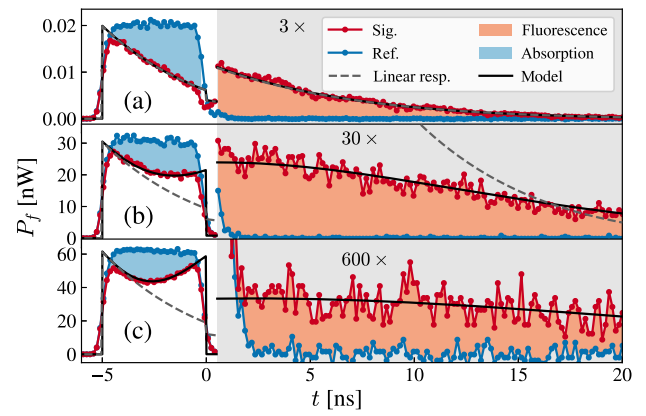

FIG. 2. Dynamics of the power of a fiber-guided, resonant 5 ns probe pulse transmitted through about 300 atoms for different input powers (red dots). The reference measurement without atoms is shown as blue dots. (a) In the weak excitation regime, the dynamics is well-captured by linear response theory (gray dashed line). (b),(c) For larger powers, the dynamics deviates from linear response, but is captured by a cascaded interaction model (black solid line). We extract the number of photons absorbed and emitted into the forward propagating mode from the area of the blue and light-red shaded areas, respectively. Note the rescaled y axis for $t > 0$ ns.

smaller than the decay rate of the atoms, thus not altering the dynamics. We estimate the temperature of the cooled atoms to be about 10 μK [43,44]. Moreover, degenerate Raman cooling continuously pumps the atoms to the outermost Zeeman ground state, $|g\rangle = |6S_{1/2}, F = 4, m_F = -4\rangle$. In order to study the collective dynamics, we launch probe light pulses into the fiber, which are resonant with the $|6S_{1/2}, F = 4\rangle \rightarrow |6P_{3/2}, F = 5\rangle$ D2 transition. At the position of the atoms, the probe light is almost perfectly σ^--polarized [45]. The pulses thus predominantly drive the cycling transition between ground state $|g\rangle$ and excited state $|e\rangle = |6P_{3/2}, F = 5, m_F = -5\rangle$, realizing a two-level atom. We derive the probe pulses from a continuous wave laser using two cascaded Mach-Zehnder–based amplitude modulators. For all measurements, the pulse length is set to $T_{\text{pulse}} = 5$ ns, i.e. much shorter than the $6P_{3/2}$ state's natural lifetime of about 30.5 ns [46]. Per sequence, we launch 400 probe pulses into the nanofiber (repetition rate 5 kHz) and record time traces of the output power in both forward and backward direction using single-photon counting modules; see Supplemental Material (SM) [44]. The number of trapped atoms stays essentially constant during this probing (we measure that at most 15% are lost). To obtain sufficient statistics, we average several hundred recorded traces.

Figure 2 shows time traces (red dots) of the measured output power in the forward direction, P_f, for different input pulse powers and about 300 trapped atoms. For comparison, we also show P_f without atoms (blue dots), as well as the prediction of linear response theory, which models the atoms as classical Lorentz oscillators (gray dashed line) [33]. For the input probe power of 20 pW in Fig. 2(a), we observe that P_f decreases during the excitation pulse as predicted by linear response. Subsequently, the atoms emit fluorescence into the waveguide with a

collectively enhanced decay constant of 6.1(1) ns [33]. When we increase the input power by about 3 orders of magnitude to 30 nW and 60 nW in Figs. 2(b) and 2(c), respectively, the dynamics deviates from linear response. Generally, the strength of the optical drive can be quantified by the Rabi frequency seen by the first atom

$$\Omega_1 = \sqrt{\frac{4\beta_f \Gamma P_1}{\hbar\omega}}, \qquad (1)$$

where P_1 is the optical input probe power, $\hbar\omega$ the photon energy, and $\beta_f = \Gamma_f/\Gamma \approx 0.01$ the coupling strength to the forward-propagating mode [44]. Here, Γ_f is the emission rate into the forward-propagating mode and Γ is the total emission rate. The coupling strength β_f, which is determined by the overlap integral of the atomic radiation mode and the forward-propagating guided mode gives the probability that a single, excited atom emits a photon into the guided mode. The pulse area seen by the first atom is $A_1 = \Omega_1 T_{\text{pulse}} \approx 0.02\pi$ in Fig. 2(a), i.e., much smaller than π. Therefore, the atoms reside mostly in their ground state, and the dynamics can be described by linear response theory. The pulse areas in Figs. 2(b) and 2(c) are about 0.7π and π, respectively, such that the atomic nonlinearity becomes apparent. The observed nonlinear transmission dynamics during the excitation pulse results from Rabi oscillations of the atomic ensemble, which manifests as a modulation of the coherently reradiated field. In particular, during the excitation pulse we observe an increase of P_f after an initial decrease in Fig. 2(c) as the ensemble

becomes transparent when it is fully inverted. The fluorescence power for $t > 0$ ns is orders of magnitude lower than predicted by linear response in Figs. 2(b) and 2(c).

Let us now try to understand the observed nonlinear dynamics quantitatively. Because of the chiral coupling of the atoms to the nanofiber mode, the σ^--polarized fluorescence is predominantly emitted into the forward direction [47], which is why we neglect the optical drive from the backward-propagating mode in the following. We thus describe our system using a cascaded interaction model; see Fig. 1(b). We neglect free-space coupling between the atoms because their average nearest-neighbor distance exceeds half the free-space wavelength of the emitted radiation. We describe the kth atom by the density operator $\hat{\rho}_k$ and assume that it is driven by a coherent, time-dependent field with amplitude α_k. The first atom is driven by the field $\alpha_1 = \sqrt{P_1/(\hbar\omega)}$. We determine α_{k+1} by interfering α_k with the coherent part of the light field that is emitted into the waveguide by the kth atom, yielding the input-output equation [48]

$$\alpha_{k+1} = \alpha_k - i\sqrt{\beta_f \Gamma} \rho_k^{ge}. \tag{2}$$

Consecutively solving the Lindblad master equation for each atom and Eq. (2) for all fields, we obtain the time-dependent quantities α_k, ρ_k^{ge}, and ρ_k^{ee} and compute the transmitted power, P_f, via

$$P_f = \hbar\omega \left[|\alpha_{N+1}|^2 + \beta_f \Gamma \sum_{k=1}^{N} (\rho_k^{ee} - |\rho_k^{eg}|^2) \right]. \tag{3}$$

As can be seen from Eq. (3), P_f generally differs from $\hbar\omega|\alpha_{N+1}|^2$, i.e., the field is not in a coherent state anymore. The first term in the square bracket thus describes the coherent part of the transmitted radiation while the second term describes the incoherently emitted light. While this incoherent part does contribute to the total emitted power, we neglect the stimulation of emission by it, such that it does not influence the dynamics of the downstream atoms. Our model is equivalent to a time-dependent first-order cumulant expansion [49] and coincides with linear response theory in the limit of weak excitation [33]. For large ensembles in a perfectly inverted state, higher-order correlations have to be included to correctly describe the dynamics [49]. To account for temperature-induced fluctuations of the atomic positions and the corresponding coupling strengths, we draw β_f from a Gaussian distribution; see SM for details [44]. By fitting the simulated P_f to our experimental data, we find the mean and standard deviation of β_f to be 0.0108 and 0.0065, respectively. This mean value agrees reasonably with an independent saturation measurement [42] that yields $\beta_f = 0.009(1)$. We numerically checked that this spread of β_f does not

qualitatively alter the collective dynamics [44,50]. The predicted power according to Eq. (3) is shown as black solid lines in Fig. 2. In the weak excitation regime, it reproduces the predictions of linear response. Remarkably, the model also describes the dynamics in the nonlinear regime well.

To further shed light on the system dynamics, we determine the absorbed pulse energy from the blue shaded areas in Fig. 2. From this, we infer the average number of absorbed photons per atom, n_{abs}, which we show in Fig. 3(a) as a function of the input power P_1 (and pulse area A_1). The black dots indicate the measured values, which are quantitatively predicted by our model (solid black line). The corresponding model prediction of the average excitation probability at $t = 0$, p_{exc}, is shown as the dashed black line in Fig. 3(a). We observe damped Rabi oscillations, where n_{abs} and p_{exc} reach maximum values of 0.85(1) and 0.76(1), respectively. We thus conclude that we achieve significant inversion of the ensemble. We note that, due to absorption of the excitation pulse along the atomic ensemble, maximal inversion is reached for a pulse area of $A_1 = 1.06\pi$, which is slightly larger than π. Because of the small probability that an atom decays during the probe pulse, p_{exc} is slightly smaller than n_{abs}. In the following, we use the experimentally obtained n_{abs} as an estimate of p_{exc}.

We now study the number of photons, n_{em}^f, that are emitted per atom into the forward direction after switching off the pulse, inferred from the light-red shaded areas in Fig. 2. Figure 3(b) shows the measured values of n_{em}^f (blue diamonds) and the corresponding model prediction (solid blue line). The maximum value of n_{em}^f is as high as 0.225(2), meaning that, on average, about 70 photons are emitted into the forward direction by 300 atoms. Notably, the maximum of n_{em}^f does not occur for the same pulse area as the maximum of p_{exc}, because n_{em}^f depends on both the collective enhancement of radiation and on the total number of photons stored in the ensemble. While the former stems from constructive interference of the scattered fields and is maximized for vanishing input power, the latter peaks for a π pulse.

In order to quantify the collective enhancement in forward emission, we compute the fraction of stored energy emitted into the forward direction, $\eta_f = n_{em}^f/n_{abs}$, shown as blue diamonds in Fig. 3(c). The solid blue line shows the corresponding model prediction. For vanishing input power, where the emission is fully coherent, the system behaves as a phased array of classical dipoles, featuring enhanced forward scattering, as predicted by linear response. The maximum value of $\eta_f = 0.62(1)$ corresponds to a sixtyfold enhancement compared to independent emission. As we increase the input power, incoherent spontaneous emission starts to dominate the decay dynamics. Concomitantly, η_f drops, reaching a minimal value of 0.011(2) for a pulse area of 1.06π. While η_f reaches a
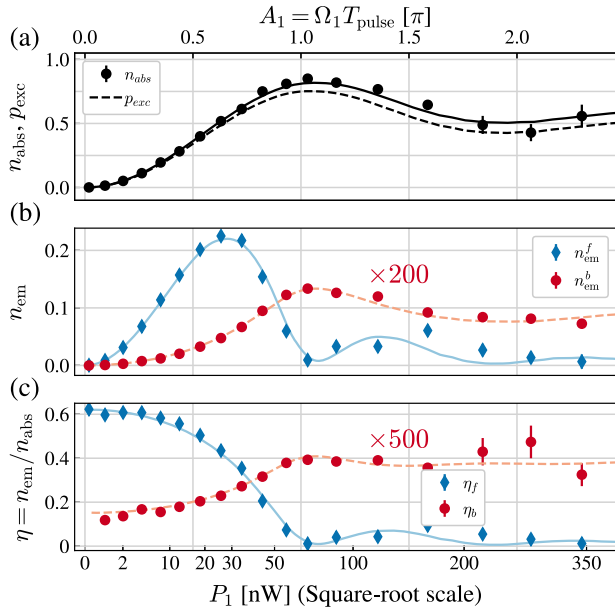
FIG. 3. (a) Measured average number of absorbed photons per atom, n_{abs}, as a function of the input power, P_1, and the corresponding pulse area seen by the first atom, A_1. The black solid and dashed lines show the model prediction for n_{abs} and the excited state probability, p_{exc}, respectively. We observe damped Rabi oscillations, where up to about 80% of the atoms are being excited. (b) Number of photons per atom emitted into the forward (backward) propagating mode, n_{em}^f (n_{em}^b), shown as blue diamonds (red dots). The corresponding model prediction is indicated by the blue solid (red dashed) line. (c) Fraction of stored energy emitted into the forward (backward) propagating mode, η_f (η_b). For weak driving, η_f is collectively enhanced. As the power is increased, η_f decreases and reaches its minimal value for a pulse area of π, while η_b follows the opposite trend.

minimal value that coincides with the value expected for independently emitting atoms, i.e., $\min(\eta_f) \approx \beta_f$, the ensemble still features collective dynamics, as can be seen from the nonexponential decay in Fig. 2(c). This reduction of η_f is due to a loss of atomic coherence, which is expected for an inverted ensemble.

In addition to P_f, we also measure the output power in the backward direction, P_b. We plot the average number of photons per atom, n_{em}^b, as well as the fraction of stored energy that is emitted into the backward direction, η_b, as red dots in Figs. 3(b) and 3(c), respectively. In contrast to the forward direction, n_{em}^b follows a similar trend as p_{exc} and peaks at a pulse area of about π. This backward emission of radiation is due to the small overlap of the atomic radiation mode with the backward-propagating mode, which we neglect in the cascaded interaction model. The expected backward coupling strength can be computed to be $\beta_b = 0.087\beta_f$ [47]. In order to estimate n_{em}^b, we incoherently sum up the time-dependent atomic emission rates to calculate the power emitted into the backward direction
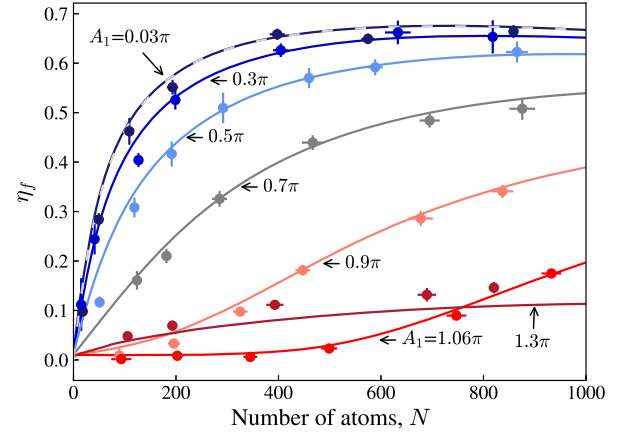

FIG. 4. Fraction of stored energy emitted into the forward direction, η_f, as a function of the atom number, N, for different pulse areas, A_1. The data are well-described by the cascaded interaction model (solid lines). As a comparison, we also plot the result from linear response theory (gray dashed line), which coincides with the prediction of the cascaded interaction model for the smallest pulse area, $A_1 = 0.03\pi$.

$$P_b = \hbar\omega \sum_{k=1}^{N} \beta_b \Gamma \rho_k^{ee}, \qquad (4)$$

which we integrate over time to obtain n_{em}^b. The assumption of incoherent summation is motivated by the fact that the spatial period of the trapping potential does not fulfill the condition for Bragg reflection of the probe light, and the atoms are randomly distributed over the trapping sites with a nonunity filling factor. Indeed, the resulting model prediction agrees quantitatively with the experimental data; see dashed red lines in Figs. 3(b) and 3(c).

To further consolidate our cascaded interaction model, we now turn to the forward emission again and study η_f as a function of the atom number, N, for different pulse areas A_1 in Fig. 4. The colored dots show the experimental data, which are well-predicted (solid lines) throughout the whole parameter range. For the smallest values of A_1, η_f first increases linearly with N and then reaches a plateau, where up to 66(2)% of the stored energy is emitted into the forward propagating mode. This behavior is captured by linear response theory (dashed gray line). Beyond this regime, both the initial slope of $\eta_f(N)$ and the value of the plateau decrease with A_1. For $A_1 = 0.9\pi$, we observe a qualitative change in the behavior of η_f, which initially increases superlinearly with N, indicative of the buildup of a collective dipole moment along the array of atoms. For $A_1 = 1.06\pi$, η_f stays at a low constant value until $N \approx 400$, from when on it increases superlinearly. We numerically checked that the initially constant $\eta_f(N)$ is due to the finite temperature of the atoms; see SM [44]. For an even larger pulse area of $A_1 = 1.3\pi$, η_f scales qualitatively similarly with N as for the case of $A_1 = 0.7\pi$. The smaller values of slope and plateau are predominantly due to the larger thermal fluctuations of the pulse areas seen by the different atoms.

In conclusion, through the unidirectional coupling of up to 1000 atoms to a nanofiber, we realized a cascaded quantum system, where the dynamics of each atom depends only on the dynamics of the upstream atoms [51,52]. We studied the coherent excitation dynamics of the atomic ensemble and confirmed that we achieve almost full inversion by counting the number of photons absorbed from the excitation pulse.

We showed that throughout a large parameter range from weak excitation to full inversion, we can simulate the dynamics with a model whose computational complexity is linear in the number of atoms and which explains how the complex interplay between collectively enhanced forward scattering and the number of excitations determine how much energy is emitted into the waveguide.

The agreement between our model and the data indicates that the coherent part of the emitted fields dominates the decay dynamics over a surprisingly wide range of parameters. Beyond the parameter regime studied here, interesting avenues for future research open up. For example, for larger numbers of fully inverted atoms, a given atom is predominantly driven by the incoherent part of the light emitted by the other atoms. In this regime, an initial buildup of the collective emission intensity has been predicted [53] and recently observed [54]. In stark contrast to the usual case of Dicke superradiant bursts [55–57], this dynamics is independent of the average separation between adjacent emitters. By tuning the directionality of atom-waveguide coupling, the dynamic mode competition in the presence of a directional bias could be studied. In this case, even a small asymmetry in the coupling strength may lead to a strongly directional emission [22]. Finally, our results constitute an important step toward full coherent optical control of atoms that interact via a nanophotonic waveguide, enabling, e.g., the generation of multiphoton quantum states of light [58,59].

[*]Corresponding author.
arno.rauschenbeutel@hu-berlin.de

[1] D. E. Chang, J. S. Douglas, A. González-Tudela, C.-L. Hung, and H. J. Kimble, Rev. Mod. Phys. **90**, 031002 (2018).

[2] L.-M. Duan, M. D. Lukin, J. I. Cirac, and P. Zoller, Nature (London) **414**, 413 (2001).

[3] D. Meiser, J. Ye, D. R. Carlson, and M. J. Holland, Phys. Rev. Lett. **102**, 163601 (2009).

[4] G. Facchinetti, S. D. Jenkins, and J. Ruostekoski, Phys. Rev. Lett. **117**, 243601 (2016).

[5] A. Asenjo-Garcia, M. Moreno-Cardoner, A. Albrecht, H. J. Kimble, and D. E. Chang, Phys. Rev. X **7**, 031024 (2017).

[6] M. O. Scully and A. A. Svidzinsky, Science **325**, 1510 (2009).

[7] W. Guerin, M. O. Araújo, and R. Kaiser, Phys. Rev. Lett. **116**, 083601 (2016).

[8] M. O. Araújo, I. Krešić, R. Kaiser, and W. Guerin, Phys. Rev. Lett. **117**, 073002 (2016).

[9] S. J. Roof, K. J. Kemp, M. D. Havey, and I. M. Sokolov, Phys. Rev. Lett. **117**, 073003 (2016).

[10] D. Das, B. Lemberger, and D. Yavuz, Phys. Rev. A **102**, 043708 (2020).

[11] T. S. do Espirito Santo, P. Weiss, A. Cipris, R. Kaiser, W. Guerin, R. Bachelard, and J. Schachenmayer, Phys. Rev. A **101**, 013617 (2020).

[12] J. Rui, D. Wei, A. Rubio-Abadal, S. Hollerith, J. Zeiher, D. M. Stamper-Kurn, C. Gross, and I. Bloch, Nature (London) **583**, 369 (2020).

[13] Y. He, L. Ji, Y. Wang, L. Qiu, J. Zhao, Y. Ma, X. Huang, S. Wu, and D. E. Chang, Phys. Rev. Lett. **125**, 213602 (2020).

[14] N. Stiesdal, H. Busche, J. Kumlin, K. Kleinbeck, H. P. Büchler, and S. Hofferberth, Phys. Rev. Res. **2**, 043339 (2020).

[15] G. Ferioli, A. Glicenstein, L. Henriet, I. Ferrier-Barbut, and A. Browaeys, Phys. Rev. X **11**, 021031 (2021).

[16] A. Cipris, N. A. Moreira, T. S. do Espirito Santo, P. Weiss, C. J. Villas-Boas, R. Kaiser, W. Guerin, and R. Bachelard, Phys. Rev. Lett. **126**, 103604 (2021).

[17] G. Ferioli, A. Glicenstein, F. Robicheaux, R. T. Sutherland, A. Browaeys, and I. Ferrier-Barbut, Phys. Rev. Lett. **127**, 243602 (2021).

[18] A. Glicenstein, G. Ferioli, A. Browaeys, and I. Ferrier-Barbut, Opt. Lett. **47**, 1541 (2022).

[19] S. J. Masson, I. Ferrier-Barbut, L. A. Orozco, A. Browaeys, and A. Asenjo-Garcia, Phys. Rev. Lett. **125**, 263601 (2020).

[20] S. J. Masson and A. Asenjo-Garcia, Nat. Commun. **13**, 1 (2022).

[21] E. Sierra, S. J. Masson, and A. Asenjo-Garcia, Phys. Rev. Res. **4**, 023207 (2022).

[22] F. Robicheaux, Phys. Rev. A **104**, 063706 (2021).

[23] O. Rubies-Bigorda and S. F. Yelin, Phys. Rev. A **106**, 053717 (2021).

[24] B. Lemberger and K. Mølmer, Phys. Rev. A **103**, 033713 (2021).

[25] D. Plankensteiner, C. Hotter, and H. Ritsch, Quantum **6**, 617 (2022).

[26] K. P. Nayak, M. Sadgrove, R. Yalla, F. Le Kien, and K. Hakuta, J. Opt. **20**, 073001 (2018).

[27] A. S. Sheremet, M. I. Petrov, I. V. Iorsh, A. V. Poshakinskiy, and A. N. Poddubny, Rev. Mod. Phys. **95**, 015002 (2023).

[28] A. Goban, C.-L. Hung, J. D. Hood, S.-P. Yu, J. A. Muniz, O. Painter, and H. J. Kimble, Phys. Rev. Lett. **115**, 063601 (2015).

[29] P. Solano, P. Barberis-Blostein, F. K. Fatemi, L. A. Orozco, and S. L. Rolston, Nat. Commun. **8**, 1 (2017).

[30] N. V. Corzo, J. Raskop, A. Chandra, A. S. Sheremet, B. Gouraud, and J. Laurat, Nature (London) **566,** 359 (2019).

[31] S. Okaba, D. Yu, L. Vincetti, F. Benabid, and H. Katori, Commun. Phys. **2,** 1 (2019).

[32] R. Pennetta, D. Lechner, M. Blaha, A. Rauschenbeutel, P. Schneeweiss, and J. Volz, Phys. Rev. Lett. **128,** 203601 (2022).

[33] R. Pennetta, M. Blaha, A. Johnson, D. Lechner, P. Schneeweiss, J. Volz, and A. Rauschenbeutel, Phys. Rev. Lett. **128,** 073601 (2022).

[34] P. Lodahl, S. Mahmoodian, S. Stobbe, A. Rauschenbeutel, P. Schneeweiss, J. Volz, H. Pichler, and P. Zoller, Nature (London) **541,** 473 (2017).

[35] F. Le Kien, S. D. Gupta, K. P. Nayak, and K. Hakuta, Phys. Rev. A **72,** 063815 (2005).

[36] H. Zoubi and H. Ritsch, Europhys. Lett. **90,** 23001 (2010).

[37] E. Shahmoon and G. Kurizki, Phys. Rev. A **87,** 033831 (2013).

[38] C. Gonzalez-Ballestero, A. Gonzalez-Tudela, F. J. Garcia-Vidal, and E. Moreno, Phys. Rev. B **92,** 155304 (2015).

[39] S. B. Markussen, J. Appel, C. Østfeldt, J.-B. S. Béguin, E. S. Polzik, and J. H. Müller, Appl. Phys. B **126** (2020).

[40] M. Gross, C. Fabre, P. Pillet, and S. Haroche, Phys. Rev. Lett. **36,** 1035 (1976).

[41] N. Schlosser, G. Reymond, and P. Grangier, Phys. Rev. Lett. **89,** 023005 (2002).

[42] E. Vetsch, D. Reitz, G. Sagué, R. Schmidt, S. T. Dawkins, and A. Rauschenbeutel, Phys. Rev. Lett. **104,** 203603 (2010).

[43] Y. Meng, A. Dareau, P. Schneeweiss, and A. Rauschenbeutel, Phys. Rev. X **8,** 031054 (2018).

[44] See Supplemental Material at http://link.aps.org/supplemental/10.1103/PhysRevLett.130.163602 for a more detailed description of the loading of the atom trap, the detection setup, the theoretical modeling, and the influence of imperfect state preparation.

[45] F. L. Kien, J. Liang, K. Hakuta, and V. Balykin, Opt. Commun. **242,** 445 (2004).

[46] D. A. Steck, Cesium D Line Data (2019), http://steck.us/alkalidata.

[47] R. Mitsch, C. Sayrin, B. Albrecht, P. Schneeweiss, and A. Rauschenbeutel, Nat. Commun. **5,** 5713 (2014).

[48] C. W. Gardiner and M. J. Collett, Phys. Rev. A **31,** 3761 (1985).

[49] K. J. Kusmierek, S. Mahmoodian, M. Cordier, J. Hinney, A. Rauschenbeutel, M. Schemmer, P. Schneeweiss, J. Volz, and K. Hammerer, Higher-order mean-field theory of chiral waveguide QED, arXiv:2207.10439.

[50] M. S. Malcuit, J. J. Maki, D. J. Simkin, and R. W. Boyd, Phys. Rev. Lett. **59,** 1189 (1987).

[51] C. W. Gardiner, Phys. Rev. Lett. **70,** 2269 (1993).

[52] H. J. Carmichael, Phys. Rev. Lett. **70,** 2273 (1993).

[53] F. L. Kien and K. Hakuta, Phys. Rev. A **77,** 013801 (2008).

[54] C. Liedl, F. Tebbenjohanns, C. Bach, S. Pucher, A. Rauschenbeutel, and P. Schneeweiss, arXiv:2211.08940.

[55] R. H. Dicke, Phys. Rev. **93,** 99 (1954).

[56] N. Skribanowitz, I. Herman, J. MacGillivray, and M. Feld, Phys. Rev. Lett. **30,** 309 (1973).

[57] M. Gross and S. Haroche, Phys. Rep. **93,** 301 (1982).

[58] A. González-Tudela, V. Paulisch, D. E. Chang, H. J. Kimble, and J. I. Cirac, Phys. Rev. Lett. **115,** 163603 (2015).

[59] S. Mahmoodian, G. Calajó, D. E. Chang, K. Hammerer, and A. S. Sørensen, Phys. Rev. X **10,** 031011 (2020).